Applied Catalysis B: Environmental 163 (2015) 564–572

Contents lists available at ScienceDirect

Applied Catalysis B: Environmental

journal homepage: www.elsevier.com/locate/apcatb

A facile way to synthesize Ag@AgBr cubic cages with efficient visible-light-induced photocatalytic activity

Xinlai Xiao[a,b], Lei Ge[a,b,*], Changcun Han[b], Yujing Li[b], Zhen Zhao[a], Yongji Xin[b], Siman Fang[b], Linen Wu[b], Ping Qiu[b]

[a] State Key Laboratory of Heavy Oil Processing, China University of Petroleum Beijing, No. 18 Fuxue Rd., Beijing 102249, PR China
[b] Department of Materials Science and Engineering, College of Science, China University of Petroleum Beijing, No. 18 Fuxue Rd., Beijing 102249, PR China

ARTICLE INFO

Article history:
Received 15 June 2014
Received in revised form 17 August 2014
Accepted 21 August 2014
Available online 29 August 2014

Keywords:
Photocatalysis
Ag@AgBr
Cubic cage
Surface plasmon resonance

ABSTRACT

The novel cubic cage Ag@AgBr plasmonic photocatalysts were first synthesized via a water soluble sacrificial salt-crystal-template (SCT) process. This is achieved by the photo-reduction process was used to produce Ag nanoparticles on the surface of AgBr. The physical and photophysical properties of the as-prepared Ag@AgBr cubic cages were characterized by X-ray diffraction (XRD), scanning electron microscopy (SEM), transmission electron microscope (TEM), energy dispersive spectroscopy (EDS), ultraviolet–visible diffuse reflection spectroscopy (DRS), X-ray photoelectron spectroscopy (XPS), electron spin resonance (ESR) and photoluminescence spectroscopy (PL). The results showed that Ag@AgBr cubic cages have excellent photocatalytic performance under visible light illumination, since the methyl orange (MO) dyes were completely degraded within 80 s over Ag@AgBr photocatalysts and the photocatalytic activity maintains a high level after 7 cycles. A possible catalytic mechanism for Ag@AgBr cubic cages is proposed which is attributed to the surface plasmon resonance (SPR) effect from Ag and hybrid effect from AgBr.

1. Introduction

The solar energy driven water splitting and pollutants degradation through semiconductor photocatalysis is of great importance as it is a promising technique for renewable energy production and environment purification [1–6]. Photocatalysts are usually solid semiconductors with the following characteristics: (i) absorbing visible and/or UV light; (ii) chemically and biologically inert and photostable; (iii) high activity and (iv) nontoxic. Among various semiconductor photocatalysts, TiO_2 is considered as one of the most promising photocatalysts [7,8]. However, TiO_2 could only respond to photons with wavelength in UV range which absorbs only about 4% of solar energy and thus limits its application to a great extent [9–11]. Therefore, the development of simple, efficient, and sustainable photocatalysts that work well under visible light irradiation is a major challenge in this field.

To date, the explorations of highly active photocatalysts with nanostructures for solar light absorption still restrain their practical applications. It is well-known that well-controlled hierarchical structures, particularly 3D structures, could provide high specific surface area with well aligned pore structures that shorten the diffusion paths of charge carriers to active surface sites [12–15]. For example, the hierarchical structures of green leaves in certain photosynthetic plants are optimized for efficient light harvesting and sunlight conversion to chemical energy by photosynthesis process [16]. For photocatalytic or photovoltaic applications, similar structures can provide a strategy to improve photo-energy conversion efficiency due to the enhanced light harvesting, short charge-carrier transport paths, and increased active sites in porous micro/nano-channels [17–19].

Silver halide (AgBr) has been considered to be a new visible light photocatalytic material for its good sensitivity to light. For application, AgBr is usually loaded on other materials to enhance its catalytic properties [20–26]. However, AgBr rarely plays a main role in these catalysts, resulting in imperfect catalytic efficiency. By employing the SPR on noble metal nanoparticles, some highly efficient visible light response plasmonic photocatalysts have been developed. For example, Farnood et al. [27] prepared AgBr/Y-zeolite composite photocatalyst, which is highly efficient under sunlight

* Corresponding author at: State Key Laboratory of Heavy Oil Processing, China University of Petroleum Beijing, No. 18 Fuxue Road, Beijing102249, PR China. Tel.: +86 1089739096; fax: +86 1089739096.
E-mail address: gelei08@sina.com (L. Ge).

http://dx.doi.org/10.1016/j.apcatb.2014.08.037
0926-3373/

irradiation, but it is too unstable for practical application. Recently, some other visible-light-induced photocatalysts, such as Ag@AgCl and Ag@AgBr have been explored [28–32]. These catalysts display high photocatalytic activity and stability under visible light irradiation due to the SPR of silver nanoparticles produced on the surface of silver halide [33,34]. However, the well controlled synthesis of Ag@AgX nanostructures still remains a challenge. To the best of our knowledge, only few attempts have been conducted on the synthesis of nanostructured Ag@AgBr with well-defined shapes. The methodological investigation of Ag@AgBr nanoparticles with novel shapes is assumed to pave the way to create efficient visible-light-induced photocatalysts.

Herein, a facile approach was developed for the first time to synthesize the 3D structure and physical stable Ag@AgBr cubic cage photocatalyst with SPR effect. The obtained AgBr shows a cubic cage structure and the Ag nanoparticles are formed in situ on AgBr surface via a photo-reduction process. Furthermore, the compositions, microstructures and photocatalytic performance of the as-obtained hierarchical photocatalysts were carefully investigated. The possible mechanisms for the formation of cubic cages and the enhanced photocatalytic performance were also investigated in detail. The outstanding properties associated with the Ag@AgBr cubic cage structures suggested that they can be used as a novel light harvesting catalyst for given applications in heterogeneous photocatalysis.

2. Experimental

2.1. Materials

Silver nitrate ($AgNO_3$, Sigma–Aldrich, 99%), potassium bromide (KBr, 99.5% A.R.), polyvinylpyrrolidone (PVP, Sigma–Aldrich, K29-32, average Mw = 58,000), absolute ethyl alcohol (EtOH, A.R.), methyl orange (MO, A.R.), rhodamine B (Rh B, A.R.) were used as received without additional purification or treatment. Milli-Q water was used as the solvent for all of the solutions or dispersions.

2.2. Synthesis of the photocatalyst

The KBr/AgBr cubic cages were prepared in the following process: first, the AgBr cubic cages were synthesized by the water soluble sacrificial salt crystal template process [35]. In a typical procedure, $AgNO_3$ ethanol solution was prepared by dissolving 1 mmol $AgNO_3$ and 1200 mg polyvinylpyrrolidone K29-32 (PVP) in 20 ml absolute ethyl alcohol. KBr saturated aqueous solution was also prepared in advance. Then, KBr saturated aqueous solution (4 ml) was injected into 100 ml absolute ethyl alcohol solution under constant vigorous stirring, and a white suspension can be observed immediately. Subsequently, 20 ml $AgNO_3$ ethanol solution was poured into the KBr ethanol dispersion. The mixture was vigorously stirred for 24 h at 0 °C, and the KBr@AgBr core–shell cubic cage were obtained.

The Ag nanoparticles (NPs) were generated on the surface of AgBr by the method of photo-reduction (PR). The KBr/AgBr ethanol dispersion was illuminated using solar simulator 300 W Xe lamp (PLS-SXE300, Beijing Perfect light Technology Co., Ltd.) for 30 min, forming KBr/Ag@AgBr core–shell nanocubes. When the collected KBr/Ag@AgBr sample was washed with water and absolute ethyl alcohol, the Ag@AgBr cubic cage structure was generated.

For comparison, the conventional Ag@AgBr particles without well-defined morphology were synthesized by ion exchange method. In a typical procedure, $AgNO_3$ solution was prepared in advance by dissolving $AgNO_3$ (1 mmol) in Milli-Q water and KBr saturated aqueous solution was also prepared in advance. After which, $AgNO_3$ solution (20 ml) was poured into the KBr saturated aqueous solution and the mixture was vigorously stirred for 2 h, forming conventional AgBr. Ag nanoparticles were generated on the surface of AgBr by photo-reduction, detailed procedure as described above.

2.3. Characterization

The crystal structure of the sample was investigated using X-ray diffraction (XRD; Bruker D8 Advance, X-ray diffractometer) with CuKα radiation at a scan rate of $3^\circ\,min^{-1}$. The acceleration voltage and the applied current were 40 kV and 40 mA, respectively. The morphology of the samples was examined by field emission scanning electronic microscope (FESEM, FEI Quanta 200F, accelerating voltage 20 kV) and high-resolution transmission electron microscopy (HRTEM, JEM-2100, accelerating voltage 200 kV). UV–vis diffuse reflection spectroscopy (DRS) was performed on a Shimadzu UV-4100 spectrophotometer using $BaSO_4$ as the reference material. The XPS was measured in a PHI 5300 ESCA system. The beam voltage was 3.0 eV, and the energy of Ar ion beam was 1.0 keV. The binding energies were normalized to the signal for adventitious carbon at 284.8 eV. The PL spectra of the photocatalysts were detected using a Varian Cary Eclipse spectrometer with excitation wavelength of 325 nm.

The ESR signals of spin-trapped oxidative radicals were obtained on a Bruker model ESR JES-FA200 spectrometer equipped with a quanta-Ray Nd:YAG laser system as the light source with a UV-cutoff filter ($\lambda \geq 400$ nm). The ESR technique is normally used to detect radicals in reaction systems. DMPO (5,5-dimethyl-1-pyrroline-N-oxide) is a nitrone spin trap generally used for trapping radicals due to the generation of stable free radicals, DMPO–•OH or DMPO–O_2•$^-$. DMPO can produce an adduct with hyperfine splitting due to both the β-hydrogen and the nitroxide, and can be used as a radical scavenger.

2.4. Photocatalytic activity

The photocatalytic activities of the as-prepared samples were evaluated by photo-degradation of the MO and rhodamine B (RhB) dyes in aqueous solution under visible-light irradiation. All the experiments were conducted in ambient conditions. In a typical experiment, 100 mg photocatalyst powder was suspended in 100 ml MO (or RhB) aqueous solution ($10\,mg\,L^{-1}$). The solution was pre-stirred vigorously in the dark for 60 min to establish adsorption–desorption equilibrium. After that, a solar simulator 300 W Xe lamp coupled with a UV-cutoff filter (400 nm) was used as the visible light source to irradiate the suspension under vigorous stirring. The light intensity employed was $72\,mW\,cm^{-2}$. The distance between the bottom surface of the Xe lamp and the top surface of the solution surface was kept at a constant of 200 mm. Samples were collected from the reaction mixture every 20 s. Aliquots of solutions (3 ml) were drawn out from the reaction system at given degradation durations (i.e., 1 min). The suspensions sampled were centrifuged twice at 9000 rpm for 5 min to separate the solid photocatalyst particles completely, and the top transparent solutions obtained were then transferred to a quartz curette to measure their absorption spectra in a wavelength range of 350–800 nm. The degradation percentage is reported as C/C_0, where C_0 is the initial concentrations of MO and RhB dyes, and C represents the corresponding concentration at a certain time interval. The relative concentrations (C/C_0) of the MO and RhB aq. solutions were determined by the absorbance (A/A_0) at 464 nm and 554 nm, respectively. Additionally, Ag@AgBr cubic cage samples after the above-mentioned first cycle experiment were centrifuged

and collected for subsequent recycling tests. All procedures for the recycling test are the same as the first cycle.

3. Results and discussion

3.1. Synthesis and characterization of Ag@AgBr cubic cage samples

The design strategy was shown in Scheme 1. A water soluble sacrificial salt-crystal-template process was used to synthesize Ag@AgBr plasmonic photocatalysts with cubic cage morphology. The KBr templates were first prepared by injecting saturated KBr aqueous solution into absolute ethyl alcohol at 0 °C The KBr solubility decreased rapidly from water (25 °C) to absolute ethyl alcohol (0 °C). Then the white colored KBr crystals were precipitated out immediately. The $AgNO_3$ solution was subsequently added into the KBr dispersions, along with the assistance of surfactant PVP to prevent the aggregation of AgBr particles. Ion exchange diffusion reaction between KBr and Ag^+ in the solution led to the heterogeneous nucleation and continued growth of AgBr on the surface of the KBr template. After 24 h reaction kept at 0 °C, the KBr/AgBr ethanol dispersion was illuminated using solar simulator 300 W Xe lamp for 30 min, forming KBr/Ag@AgBr core–shell cubes. The obtained KBr/Ag@AgBr sample was washed with water and then absolute ethyl alcohol to remove and dissolve the inside KBr template, and the final Ag@AgBr cubic cage structures were collected.

Fig. 1 illustrates the XRD patterns of Ag@AgBr photocatalysts before and after irradiating by UV–visible light. As Fig. 1A shows, the AgBr cubic cages, synthesized via a water soluble sacrificial salt-crystal-template process, can be indexed to a cubic phase (space group: Fm3m) according to the JCPDS card No. 06-0438. As shown in Fig. 1B, the Ag@AgBr composite sample, obtained by photo-reducing AgBr under UV–visible light for 30 min, exhibits a coexistence of both AgBr and Ag phases (JCPDS No. 04-0783, group space: Fm3m), where main diffraction peak of Ag exhibits at $2\theta = 38.1°$ (Fig. 1C, inset). While the AgBr sample before light irradiation can only match with JCPDS No.06-0438. The results indicate that Ag nanoparticles generate on the surface of AgBr cubic sample via photo-reduction process.

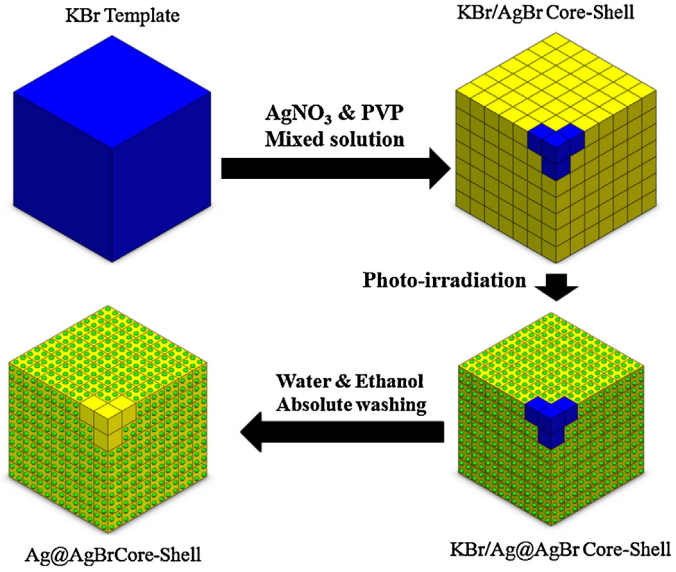

Scheme 1. Schematic illustration of the formation route of Ag@AgBr cubic cage photocatalysts.

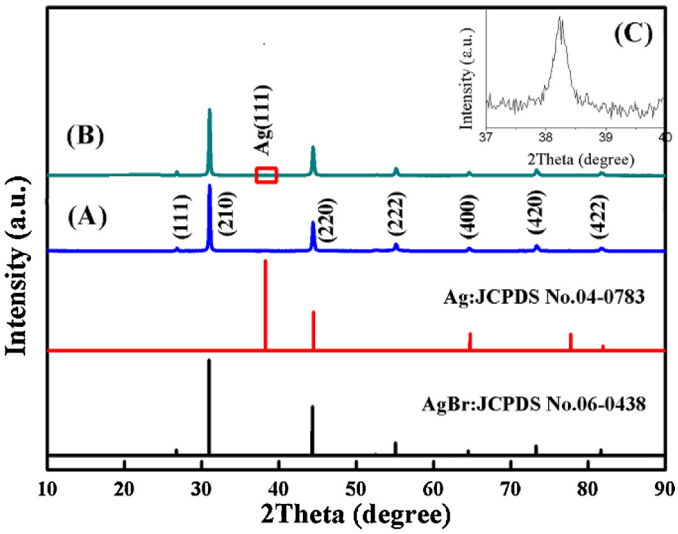

Fig. 1. XRD patterns of as-prepared samples: (A) AgBr core–shell cubes, (B) Ag@AgBr core–shell cubes, (C) inset: enlarged XRD patterns at peak position of (1 1 1) plane of cubic-phase Ag^0.

To further confirm the existence of metallic Ag species, the XPS technique was applied to determine the chemical states and surface element composition in the Ag/AgBr photocatalysts. Fig. 2 gives the XPS spectra of the as-prepared Ag@AgBr cubic cages. The survey-scan spectrum in Fig. 2A indicates that the sample consists mainly of the elements Ag and Br, besides a small amount of C. The obvious C 1s peak mainly belongs to the PVP molecules and the carbon attaching on the sample powders during the XPS measurement. Fig. 2B displays the Ag 3d XPS spectrum of the as-prepared sample. The fitted Ag 3d peaks indicate that two components coexist in Ag $3d_{5/2}$ and Ag $3d_{3/2}$ signals, giving peaks at 367.2 and 368.2 eV for $3d_{5/2}$, as well as 373.2 and 374.0 eV for Ag $3d_{3/2}$. The peaks at 367.2 and 373.2 eV can be attributed to Ag^+ species, whereas the peaks at 368.2 and 374.0 eV can be ascribed to Ag^0 species, according to previous reports [36–38]. The spectra of Br 3d (Fig. 2C) demonstrates that the binding energies of Br $3d_{5/2}$ and Br $3d_{3/2}$ are 67.8 and 68.8 eV respectively. The XPS results confirm the existence of metallic Ag^0 species in Ag@AgBr cubic cages, consistent with the XRD results.

The typical SEM and TEM images of the Ag@AgBr cubic cages are shown in Fig. 3. Fig. 3A presents the morphology of the AgBr sample before irradiation. It is observed that the AgBr sample is synthesized with well-defined cubic morphology and the average size is about 2 μm. The surface of AgBr is clean and smooth; and the inset is the high-magnification SEM image, in which barely silver nanoparticles are distributed uniformly on the surface of the as-prepared samples. It can be clearly seen from Fig. 3C that each shell wall has relatively constant shell thickness with smooth outer and inner surfaces. The shell wall thickness is estimated from Fig. 3C to be ca. 12% of the cube edge length. Fig. 3B shows the morphology of the composite Ag@AgBr cubic cages after irradiating under UV–visible light for 30 min. It can be seen that the surface of the AgBr is not clean. The inset is the high-magnification SEM image, in which it can be found that metallic silver nanoparticles are distributed uniformly on the surface of the as-prepared AgBr cubic cages. It is also clearly seen from Fig. 3D that there are some silver nanoparticles adhered to the surface of AgBr. Based on the fact that there is metallic Ag on the Ag@AgBr cubic cage sample from the XRD, XPS and SEM results, this imply that the metallic Ag particles have been in situ reduced on the surface of AgBr during synthetic process.

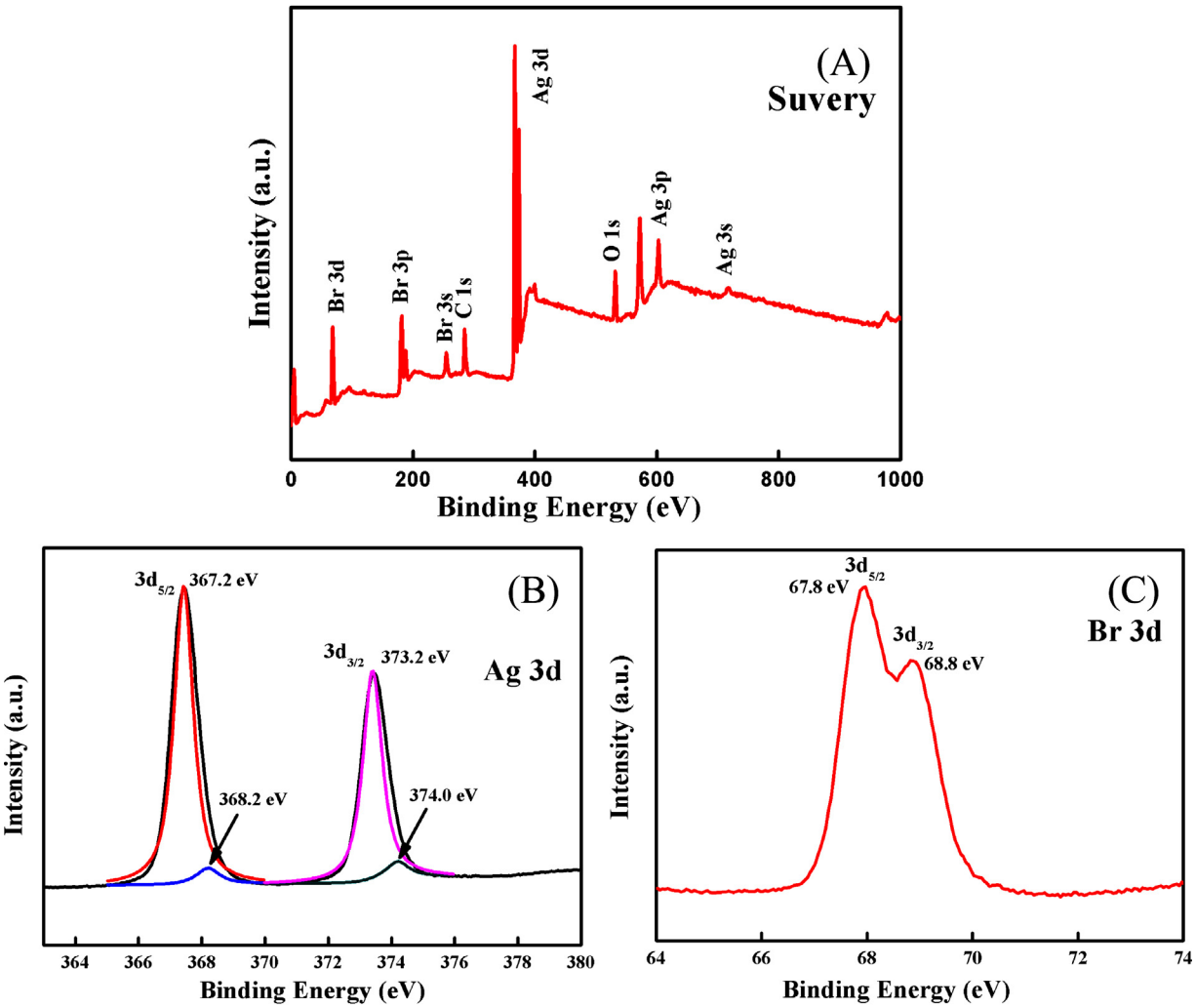

Fig. 2. The XPS spectra of the Ag@AgBr cubic cage: (A) the survey spectra, (B) Ag 3d, (C) Br 3d.

Fig. 4 presents the SEM image of the regions where elemental mapping was performed. The green and red colors in Fig. 4 correspond to the mapping of bromine and silver elements, respectively. It can be seen that the Ag and Br elements are uniformly distributed in the Ag@AgBr cubic cage sample. Fig. 4D shows a typical EDS of the Ag@AgBr cubic cages. There are only two elements, Ag and Br, in the sample. The signal of Cu in this spectrum is derived from the copper used to support the specimen and the signal of Au in the spectrum is coming from vacuum plasma spraying to make sample conducting.

The UV–DRS of AgBr and Ag@AgBr cubic cages are illustrated in Fig. 5. The onset of the adsorption edge for conventional Ag@AgBr sample is located at 500 nm, corresponding to the band gap of 2.48 eV. As we can see in Fig. 5C, the conventional Ag@AgBr shows a spherical structure, with the average size about 2.7 μm. Comparing with the conventional Ag@AgBr, the cubic cage Ag@AgBr sample shows a higher absorption in visible light region from 450 nm to 800 nm (Fig. 5A and B). This can be attributed to the SPR effect of silver nanoparticles deposited on AgBr cubic cages, which is a consequence of enhancement of the local electromagnetic field due to the collective response of the electrons at specific wavelengths. Therefore, the as-prepared Ag@AgBr cubic cages may have the potential to achieve high photocatalytic activity in the whole sunlight region.

3.2. Photocatalytic performance of Ag@AgBr cubic cages

The photocatalytic performance of Ag@AgBr cubic cages were explored by choosing the photodegradation of MO and RhB dyes in aqueous solution under visible light irradiation ($\lambda \geq 400$ nm) at room temperature. Fig. 6 demonstrates the photocatalytic activities of the Ag@AgBr samples under visible light illumination. The MO and RhB degradations over conventional Ag@AgBr spherical particles and N-doped TiO_2 samples were also carried out as a comparison to the Ag@AgBr cubic cage photocatalysts. The blank experiments indicated that the degradation of MO and RhB was negligible in the absence of photocatalyst.

As shown in Fig. 6A, it can be clearly seen that Ag@AgBr cubic cages exhibited excellent photocatalytic activities in the MO degradation reaction. The MO dye can be completely photodegraded within 80 s under visible-light irradiation and the peak intensity decreased rapidly at wavelengths of 480 nm (as shown in Fig. 6C), while the complete decomposition of MO dye over normal Ag@AgBr sample needed 140 s. Additionally, the experimental results for the RhB degradation under the same conditions (Fig. 6B) clearly indicated that their photoreactivity order was highly consistent with the above results for the MO degradation. The RhB dye can be completely degraded within 160 s in the presence of Ag@AgBr cubic cages. The comparison experimental results also revealed that the photocatalytic activities of Ag@AgBr cubic cages were much higher than that of N-TiO_2 and normal Ag@AgBr photocatalysts.

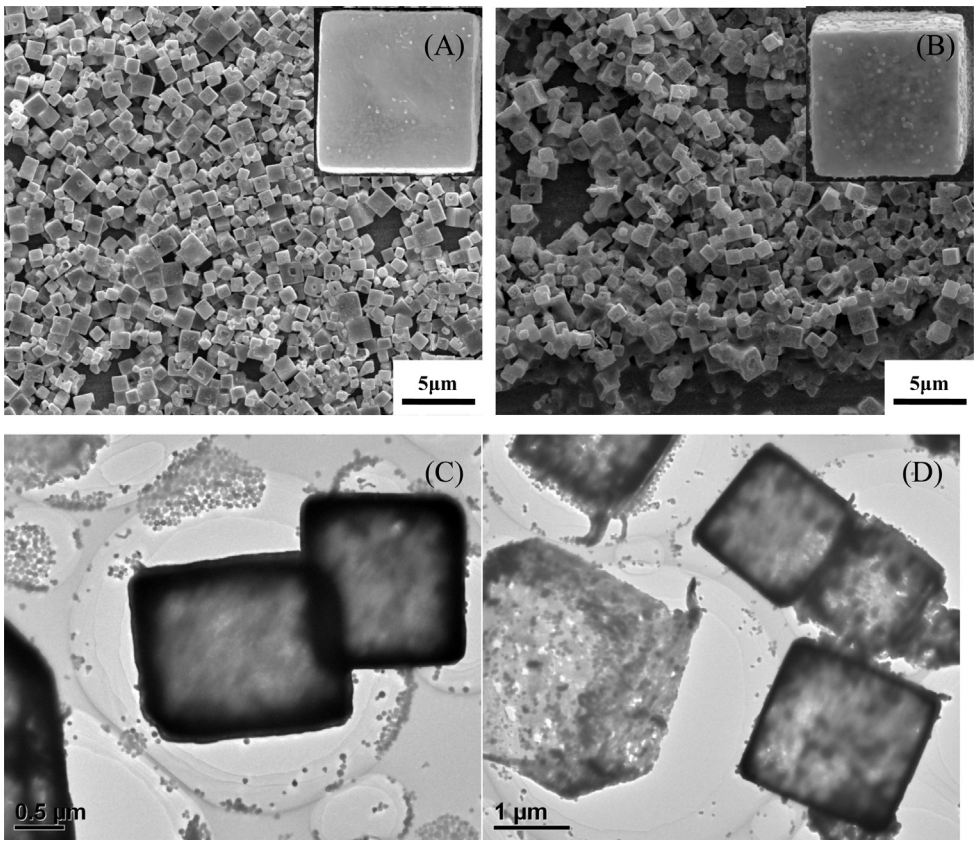

Fig. 3. (A) The typical SEM image of AgBr cubic cages, the inset on the upper right shows the high-magnification. (B) The typical SEM image of Ag@AgBr cubic cages, the inset on the upper right shows the high-magnification. (C) The typical TEM image of AgBr sample. (D) The typical TEM image of Ag@AgBr cubic cages.

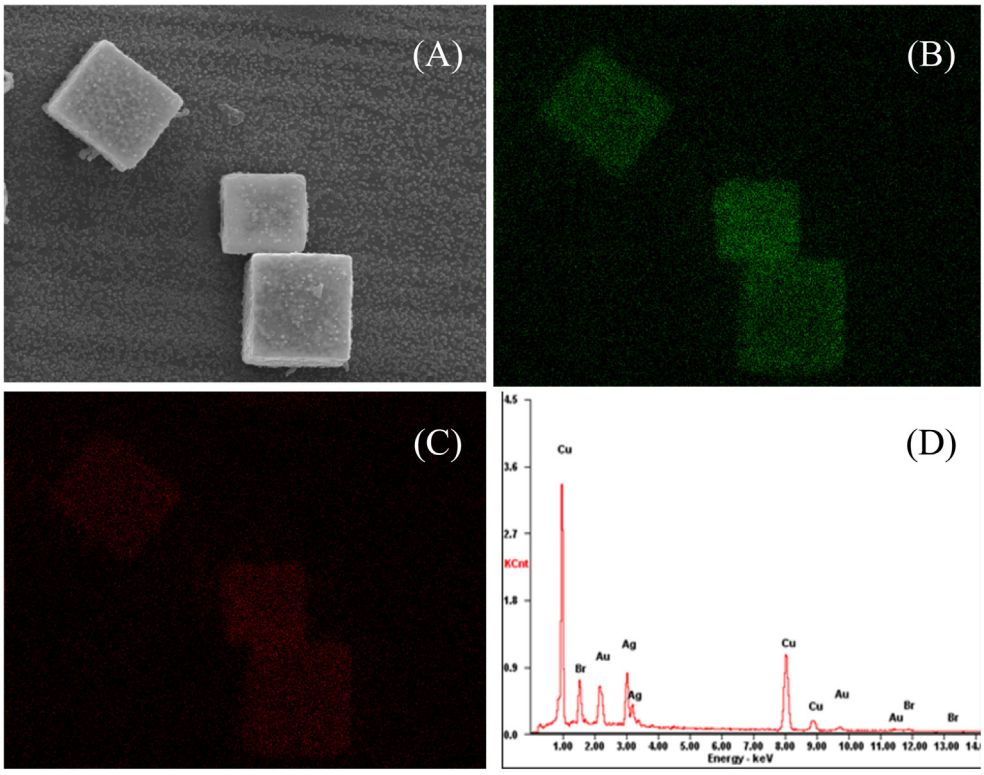

Fig. 4. Energy dispersive X-ray (EDX) elemental mapping analysis of Ag@AgBr cubic cage sample, showing the SEM image of the analyzed sample. (A) The SEM image of Ag@AgBr. (B) The green color is element Br. (C) The red color is element Ag. (D) Energy dispersive spectrometer (EDS) of Ag@AgBr cubic cages. (For interpretation of the references to color in this figure legend, the reader is referred to the web version of this article.)

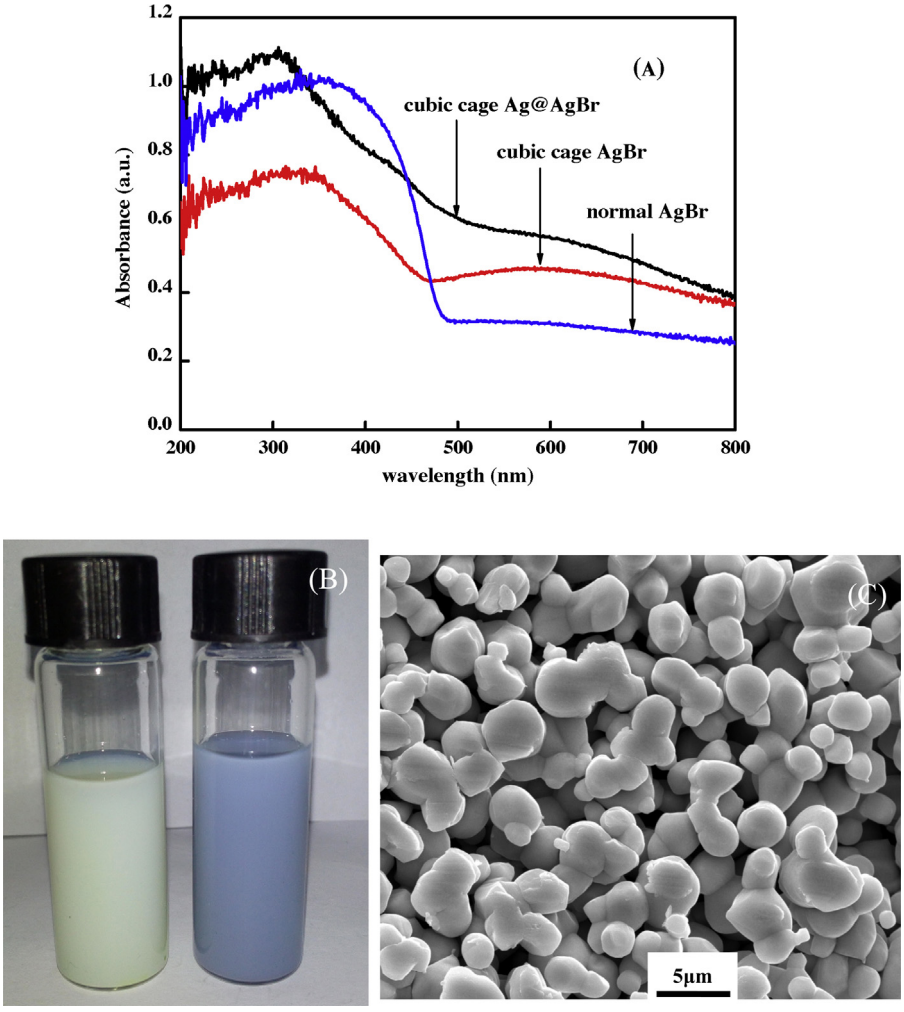

Fig. 5. (A) UV–visible diffuse reflectance spectrum of the samples: cubic cage Ag@AgBr (black line); cubic cage AgBr (red line); normal Ag@AgBr (blue line). (B) Images of AgBr (left bottle) and Ag@AgBr cubic cages (right bottle). (C) The SEM image of normal Ag@AgBr particles. (For interpretation of the references to color in this figure legend, the reader is referred to the web version of this article.)

In addition to activity, the renewable catalytic activity or stability is another important factor for evaluation. To illustrate the stability of Ag@AgBr cubic cages, the cycling catalytic performance of the Ag@AgBr cubic cage photocatalyst was performed seven times under the same conditions after centrifugal separations. As shown in Fig. 6E and F, the photocatalytic activity of the as-prepared Ag@AgBr cubic cages still maintained a high level, even though it was used 7 times for dyes degradation, indicating its sufficient stability for environment purification. After 7 cycles, the morphology of Ag@AgBr cubic cage is still in the cubic cage structure. That could be the reason of maintaining high photocatalytic activity. Moreover, the SEM images (Fig. 6G and H) also demonstrated that no obvious changes in the microstructure and morphology were observed after the cycling experiments. All these results indicated that the as-prepared Ag@AgBr cubic cage photocatalyst was highly stable.

3.3. Photocatalytic performance of Ag@AgBr cubic cages

As shown in Fig. 7A, there is no ESR signal in the dark, but a gradual evolution of ESR signals for DMPO–$O_2\bullet^-$ adducts in H_2O and DMSO is observed with visible light irradiation. The characteristic peaks with intensity similar to that of DMPO–$O_2\bullet^-$ adducts are observed only under visible light irradiation, which is consistent with the previous studies for $O_2\bullet^-$ adduct [39]. Note that the DMPO–•OH adducts were not detected in H_2O and DMSO system. Tian et al. [40] demonstrated a similar ESR result that only superoxide radical was produced by the photo-activated uniform cubic Ag@AgCl under visible light irradiation. The ESR results confirm that $O_2\bullet^-$ radicals exist in the Ag@AgBr cubic cages system under visible light irradiation, which are active oxidation species responsible for the photodegradation of organic dyes.

Combined with ESR results in Fig. 7, superoxide radical is still the main oxidative species for Ag@AgBr samples. Therefore, the efficient photocatalytic degradation of MO or RhB can smoothly proceed. To further investigate the effect of Ag NPs modification, the PL spectra of Ag@AgBr were performed. PL spectra reveal the migration, transfer, and recombination processes of the photogenerated electron–hole pairs in semiconductors. Fig. 8 presents the PL spectra of pure AgBr and the Ag@AgBr cubic cage photocatalysts at an excitation wavelength of 325 nm. At room temperature, the emission band for pure AgBr was centered at 395 nm, which was attributed to the recombination process of self-trapped excitations. The positions of the Ag@AgBr emission peaks were similar to AgBr. However, the emission intensity of Ag@AgBr photocatalyts was decreased. The result clearly indicated that recombination of photogenerated charge carriers in Ag@AgBr cubic cage was effectively restrained.

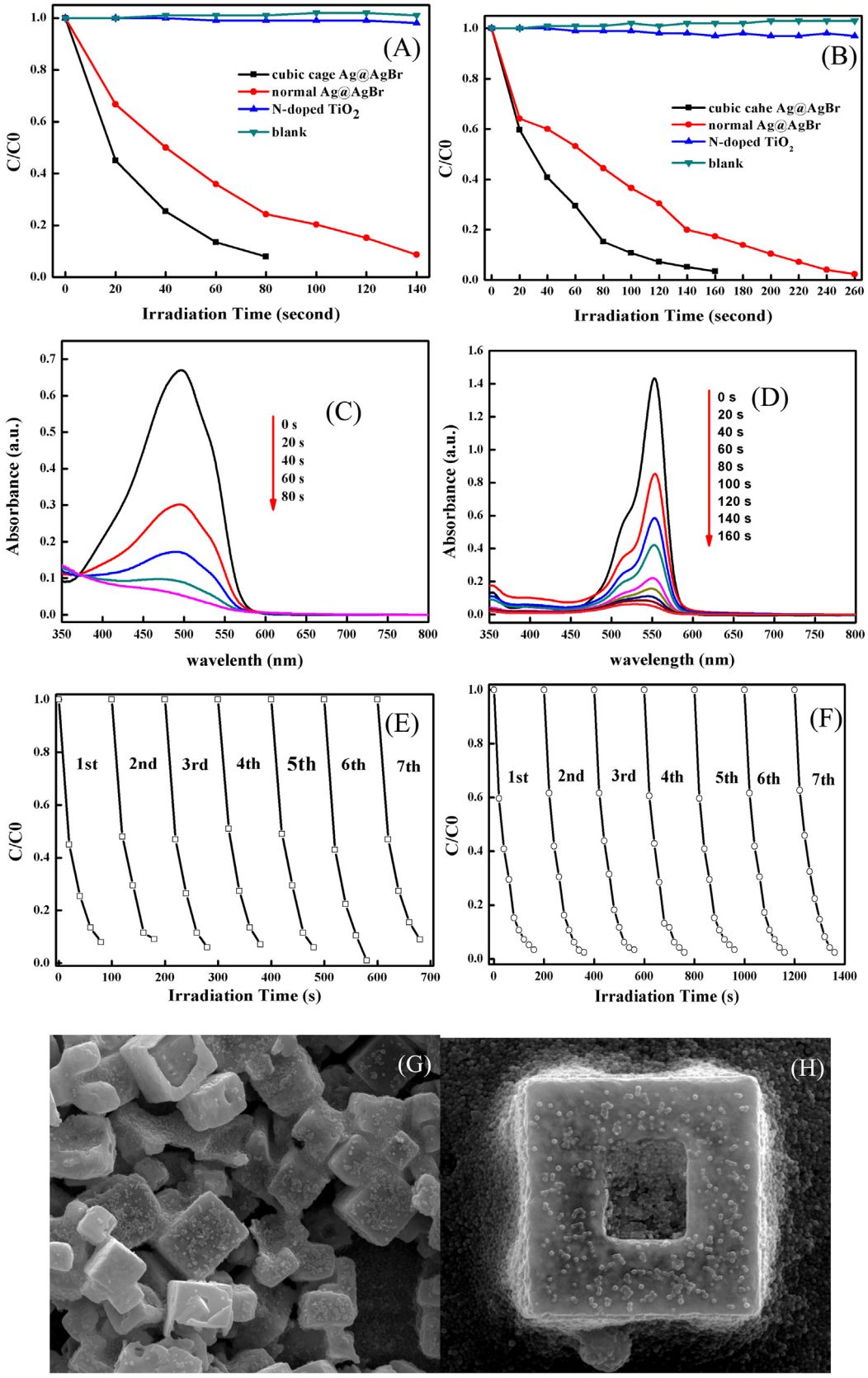

Fig. 6. (A) The degradation curves of MO over Ag@AgBr cubic cage photocatalysts; (B) the degradation curves of RhB over Ag@AgBr cubic cage photocatalysts; (C) the variations of UV–visible spectrum of MO dye vs. the corresponding degradation time; (D) the variations of UV–visible spectrum of RhB dye vs. the corresponding degradation time. (E) Cyclic photodegradation of MO solutions only in the presence of Ag@AgBr for seven cycles. (F) Cyclic photodegradation of RhB solutions only in the presence of Ag@AgBr for seven cycles; (G and H) the SEM images of Ag@AgBr after degradation.

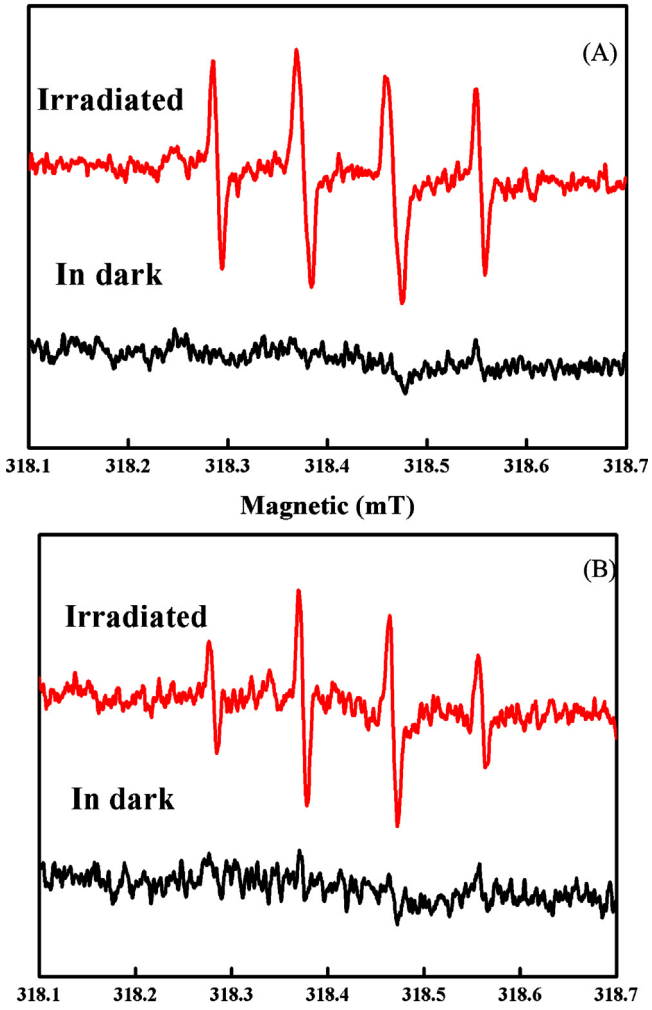

Fig. 7. ESR spectra of Ag@AgBr cubic cages in water (A) and DMSO solvents (B) under visible light irradiation ($\lambda > 420$ nm).

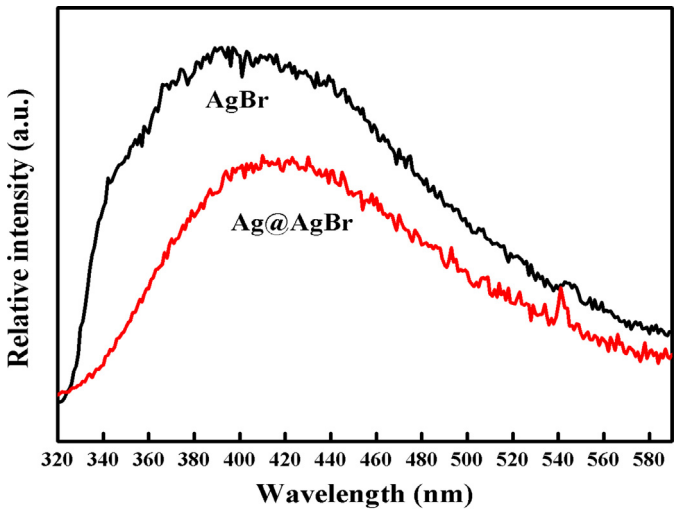

Fig. 8. Photoluminescence spectra (PL) of the AgBr and Ag@AgBr photocatalysts.

On the basis of the above results, a possible mechanism is proposed to explain the reasons to the high photocatalytic activity and stability of the as-prepared Ag@AgBr cubic cages (Fig. 9). It has been confirmed that the silver nanoparticles made great contribution to the high visible light photocatalytic activity as a result of their SPR effect produced by the collective oscillations of surface electrons. The SPR effect of silver locates at the visible light region, which leads to the strong absorption to the visible light. Additionally, the excellent conductivity of silver nanoparticles can enhance the electron migration so as to enhance the interfacial charge transfer and inhibit the recombination of electron–hole pairs efficiently. As for the Ag@AgBr cubic cages, the visible light can be absorbed efficiently by both silver nanoparticles and AgBr semiconductor. Because of the SPR induced local electromagnetic field, the separation efficiency of photogenerated charge carriers on Ag nanoparticles can be enhanced, leading to generation of a large amount of electron–hole (e^-–h^+) pairs. The well-defined interfaces facilitate the interfacial electron transfer and promote charge carrier separation, which may make another contribution to the high photocatalytic activity. On the one hand, the h^+ generated on AgBr can oxidize Br^- to Br^0, and Br^0 is the reactive radical specie and oxidizes MO or RhB dye molecules, which is consistent with the literature reported by Huang et al. [27,41,42,23,43].

Meanwhile, the noticeable behavior of electron decides the stability of as-prepared photocatalyst. Because of SPR effect of silver nanoparticles, the absorbed photon is separated into an electron and a hole. Due to the excellent conductivity of silver nanoparticles, the electron can transferred into metallic Ag particles from AgBr as far as possible rather than being trapped by the Ag^+ of AgBr, so that Ag^+ inside the AgBr cubic cages can escape from the reduction of the electrons to the maximum extent. Then these electrons go to reduce the MO or RhB molecules, or are trapped by O_2 and H_2O at the surface of photocatalyst or in the solution to form O_2^- or $O_2\bullet^-$ radicals, and other reactive oxygen species. These reactive oxygen species also help the degradation of MO or RhB dyes. These actions of electrons not only prevent the recombination of the hole and electron efficiently, but also almost avoid being captured

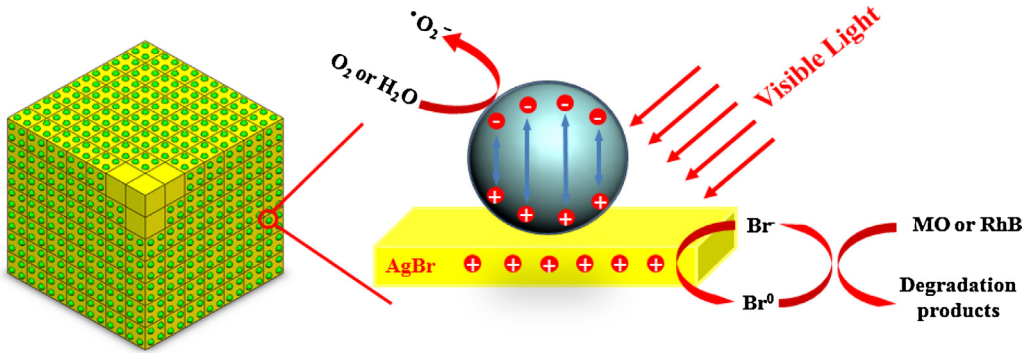

Fig. 9. Schematic diagram illustrating of the proposed degradation mechanism of organic pollutants over Ag@AgBr plasmonic photocatalyst.

by Ag^+. Meanwhile, the holes gathered on the AgBr surface caused the oxidation of Br^- ions to Br^0 atoms. As Br^0 atoms were powerful radical species, they could oxidize organic pollutants to small molecules and hence were reduced to Br^- ions again. This good cycle of bromine may be another factor in the stability of the photocatalyst. Thus, the activity is kept at a high level and, more importantly, the stability is ensured at the same time.

4. Conclusions

In summary, a stable and highly active Ag@AgBr cubic cage photocatalyst was prepared via a water soluble sacrificial salt-crystal-template process, and subsequently a photo-reduction process was used to produce Ag nanoparticles on the surface of AgBr. The as-prepared Ag@AgBr cubic cages can be used under visible light to decompose the MO dye within 80 s and degrade the RhB dye within 160 s. Moreover, the photocatalyst still keeps a high level of activity even though after 7 cycles. Radical-trapping experiments and ESR tests with DMPO confirmed that $O_2^{\bullet -}$ and Br^0 are likely to be the effective species responsible for the degradation of organics. The superiority photocatalytic performance should be attributed to both the super sensitivity of AgBr to visible light and the SPR effect of Ag nanoparticles in the region of visible light. Therefore, the novel cubic cage-like morphology, intrinsic high adsorption, and excellent photocatalytic performance of Ag@AgBr photocatalyst make it as a promising material applied in environmental purification and water disinfection.

Acknowledgements

This work was financially supported by the National Science Foundation of China (Grant Nos. 21003157 and 21273285), Beijing Nova Program (Grant No. 2008B76), and Science Foundation of China University of Petroleum, Beijing (Grant No. KYJJ2012-06-20).

References

[1] A. Kudo, Y. Miseki, Chem. Soc. Rev. 38 (2009) 253–278.
[2] Q. Zhang, D.Q. Lima, I. Lee, F. Zaera, M.F. Chi, Y.D. Yin, Angew. Chem. Int. Ed. 50 (2011) 7088–7092.
[3] H. Tong, S.X. Ouyang, Y.P. Bi, N. Umezawa, M. Oshikiri, J.H. Ye, Adv. Mater. 24 (2012) 229–251.
[4] I. Tsuji, H. Kato, A. Kudo, Angew. Chem. Int. Ed. 44 (2005) 3565–3568.
[5] D.V. Bavykin, J.M. Friedrich, F.C. Walsh, Adv. Mater. 18 (2006) 2807–2824.
[6] J.H. Mo, Y.P. Zhang, Q.J. Xu, J.J. Lamson, R.Y. Zhao, Atmos. Environ. 43 (2009) 2229–2246.
[7] X.B. Chen, S.H. Shen, L.J. Guo, S.S. Mao, Chem. Rev. 110 (2010) 6503–6570.
[8] L.G. Devi, R. Kavitha, Appl. Catal. B: Environ. 140–141 (2013) 559–587.
[9] S. Girish Kumar, L. Gomathi Devi, J. Phys. Chem. A 115 (2011) 13211–13241.
[10] I. Paramasivam, H. Jha, N. Liu, P. Schmuki, Small 8 (2012) 3073–3103.
[11] N.-G. Park, J. van de Lagemaat, A.J. Frank, J. Phys. Chem. B 104 (2000) 8989–8994.
[12] Y. Li, Z.-Y. Fu, B.-L. Su, Adv. Funct. Mater. 22 (2012) 4634–4667.
[13] S.Y. Yin, Y.Y. Zhang, J.H. Kong, C.J. Zou, C.M. Li, X.H. Lu, J. Ma, F.Y.C. Boey, X.D. Chen, ACS Nano 5 (2011) 3831–3838.
[14] Y.Y. Zhang, Y.X. Tang, S.Y. Yin, Z.Y. Zeng, H. Zhang, C.M. Li, Z.L. Dong, Z. Chen, X.D. Chen, Nanoscale 3 (2011) 4074–4077.
[15] Y. Sun, B. Mayers, Y. Xia, Adv. Mater. 15 (2003) 641–646.
[16] E. Shimoni, O. Rav-Hon, I. Ohad, V. Brumfeld, Z. Reich, Plant Cell 17 (2005) 2580–2586.
[17] J.B. Joo, Q. Zhang, I. Lee, M. Dahl, F. Zaera, Y.D. Yin, Adv. Funct. Mater. 22 (2012) 166–174.
[18] Y.X. Tang, P.X. Wee, Y.K. Lai, X.P. Wang, D.G. Gong, P.D. Kanhere, T.-T. Lim, Z.L. Dong, Z. Chen, J. Phys. Chem. C 116 (2012) 2772–2780.
[19] Y.Y. Zhang, Y.X. Tang, X.F. Liu, Z.L. Dong, H.H. Hng, Z. Chen, T.C. Sum, X.D. Chen, Small 9 (2012) 996–1002.
[20] C. Hu, T.W. Peng, X.X. Hu, Y.L. Nie, X.F. Zhou, J.H. Qu, H. He, J. Am. Chem. Soc. 132 (2010) 857–862.
[21] P.W. Huo, Y.S. Yan, S.T. Li, H.M. Li, W.H. Huang, Desalination 256 (2010) 196–200.
[22] M.R. Elahifard, S. Rahimnejad, S. Haghighi, M.R. Gholami, J. Am. Chem. Soc. 129 (2007) 9552–9553.
[23] C. Hu, Y.Q. Lan, J.H. Qu, X.X. Hu, A.M. Wang, J. Phys. Chem. B 110 (2006) 4066–4072.
[24] Y.J. Zang, R. Farnood, Appl. Catal. B: Environ. 79 (2008) 334–340.
[25] G.T. Li, K.H. Wong, X.W. Zhang, C. Hu, J.C. Yu, R.C.Y. Chan, P.K. Wong, Chemosphere 76 (2009) 1185–1191.
[26] Y.J. Zang, R. Farnood, J. Currie, Chem. Eng. Sci. 64 (2009) 2881–2886.
[27] P. Wang, B.B. Huang, X.Y. Qin, X.Y. Zhang, Y. Dai, J.Y. Wei, M.-H. Whangbo, Angew. Chem. Int. Ed. 47 (2008) 7931–7933.
[28] P. Wang, B.B. Huang, X.Y. Zhang, X.Y. Qin, H. Jin, Y. Dai, Z.Y. Wang, J.Y. Wei, J. Zhan, S.Y. Wang, J.P. Wang, M.H. Whangbo, Chem. Eur. J. 15 (2009) 1821–1824.
[29] C.H. An, S. Peng, Y.G. Sun, Adv. Mater. 22 (2010) 2570–2574.
[30] P. Wang, B.B. Huang, Z.Z. Lou, X.Y. Zhang, X.Y. Qin, Y. Dai, Z.K. Zheng, X.N. Wang, Chem. Eur. J. 16 (2010) 538–544.
[31] Y.P. Bi, J.H. Ye, Chem. Eur. J. 16 (2010) 10327–10331.
[32] T.A. El-Brolossy, T. Abdallah, M.B. Mohamed, S. Abdallah, K. Easawi, S. Negm, H. Talaat, Eur. Phys. J. Spec. Top. 153 (2008) 361–364.
[33] R.K. Roy, S. Bandyopadhyaya, A.K. Pal, Eur. Phys. J. B 39 (2004) 491–498.
[34] M.W. Chen, Y.F. Chau, D.P. Tsai, Plasmonics 3 (2008) 157–164.
[35] Y.X. Tang, Z.L. Jiang, G.H. Xing, A.R. Li, P.D. Kanhere, Y.Y. Zhang, T.C. Sum, S.Z. Li, X.D. Chen, Z.L. Dong, Z. Chen, Adv. Funct. Mater. 23 (2013) 2932–2940.
[36] P. Wang, B.B. Huang, X.Y. Zhang, X.Y. Qin, Y. Dai, Z.Y. Wang, Z.Z. Lou, ChemCatChem 3 (2011) 360–364.
[37] M.S. Zhu, P.L. Chen, M.H. Liu, ACS Nano 5 (2011) 4529–4536.
[38] M.S. Zhu, P.L. Chen, M.H. Liu, Langmuir 28 (2012) 3385–3390.
[39] L.S. Zhang, K.H. Wong, H.Y. Yip, C. Hu, J.M. Yu, C.Y. Chan, P.K. Wong, Environ. Sci. Technol. 44 (2010) 1392–1398.
[40] R.F. Dong, B.Z. Tian, C.Y. Zeng, T.Y. Li, T.T. Wang, J.L. Zhang, J. Phys. Chem. C 117 (2013) 213–220.
[41] R.C. Jin, Y.W. Cao, C.A. Mirkin, K.L. Kelly, G.C. Schatz, J.G. Zheng, Science. 294 (2001) 1901–1903.
[42] S. Link, M.A. El-Sayed, J. Phys. Chem. B 103 (1999) 8410–8426.
[43] L. Kuai, B.Y. Geng, X.T. Chen, Y.Y. Zhao, Y.C. Luo, Langmuir 26 (2010) 18723–18727.